Applied Materials Today 37 (2024) 102157

Contents lists available at ScienceDirect

Applied Materials Today

journal homepage: www.elsevier.com/locate/apmt

Piezojunction effect in heterojunctions under external bias for ultrasensitive strain sensing

Cong Thanh Nguyen [a,*], Erik W. Streed [b], Toan Dinh [a,c,d], Nam-Trung Nguyen [a], Van Thanh Dau [e], Dzung Viet Dao [a,e,*]

[a] Queensland Micro- and Nanotechnology Centre, Griffith University, Brisbane 4111, Australia
[b] Institute for Glycomics and Centre for Quantum Dynamics, Griffith University, Gold Coast 4222, Australia
[c] School of Engineering, University of Southern Queensland, Toowoomba 4350, Australia
[d] Centre for Future Materials, University of Southern Queensland, Toowoomba 4350, Australia
[e] School of Engineering and Built Environment, Griffith University, Gold Coast 4222, Australia

ARTICLE INFO

Keywords:
Piezojunction effect
Strain sensor
Gauge factor
3C-SiC/Si heterojunction
Silicon carbide
External bias

ABSTRACT

This paper investigates for the first time the piezojunction effect in heterojunctions under external bias for ultrasensitive strain sensing. As a proof of concept, we used sensing devices made of 3C-SiC/Si heterostructure with vertically aligned electrodes. Applying the beam bending method to characterize the sensing effect, the bending strain was introduced along the typical orientation [100] or [110] on (100) Si plane. Experimental results show a linear relationship between the relative change in the forward current and the applied strain from 0 to 500 ppm, decreasing under the tensile strain while increasing under the compressive strain. At the forward bias of 8 V, the obtained gauge factors (*GFs*) are 199.7 for [100] orientation and 173.1 for [110] orientation, which significantly enhance about 630 % and 540 % compared to the highest *GF* of n-type 3C-SiC in the literature. Interestingly, the *GFs* of the n^+-3C-SiC/p-Si heterostructure are positive in contrast to the negative *GFs* of n-3C-SiC thin films. The results were explained by the strain modulation on the band split and electron mass shift along the out-of-plane direction as well as by the change in the barrier height, depletion region width, and carrier concentrations under the forward bias. The ultrasensitive piezojunction effect in the 3C-SiC/Si heterojunction demonstrated in this study can pave the way toward developing ultrasensitive mechanical sensors.

1. Introduction

Strain-sensitive characteristics in semiconductors have been studied extensively for developing a wide range of mechanical sensing devices, such as pressure sensors, strain gauges, and accelerometers [1,2]. It is widely accepted that the piezoresistive effect is one of the most dominant mechanisms for making these sensors thanks to its high sensitivity, great linearity, simple fabrication, electronic integration capability, and low power consumption [3–5]. The enhancement of strain sensitivity using this sensing mechanism has attracted great attention after being discovered by Smith [6]. On the same wafer, the largest gauge factor can be obtained by selecting proper orientations, namely [100] for the n-type and [111] for the p-type (100) silicon (Si) [7,8]. Material structures also affect the piezoresistive effect. For example, single crystalline silicon carbide (SiC) has higher absolute gauge factors in comparison with polycrystalline SiC, approximately 20–30 at room temperature and about 10–18 at high temperature of 450 °C [7,9,10]. Besides, optimal doping concentrations were demonstrated to improve considerably the strain sensitivity [11,12]. Furthermore, Phan, et al. [13] experimentally demonstrated that a low density of defects was observed in SiC thin films with thicknesses more than 300 nm, which increased the gauge factor by more than 20 %. Another approach is utilizing Si nanowires thanks to advanced nanofabrication techniques [14,15]. Compared to bulk Si, the longitudinal piezoresistive coefficient of about -3550×10^{-11} Pa^{-1} in fabricated Si nanowires is about 38 times larger [15]. In this case, the increase in the charge mobility and the ratio of surface-to-volume considerably enhances the strain sensitivity.

Among all the above methods, the approach of scaling down devices to nano level has been demonstrated to enhance substantially the piezoresistive effect. However, the reliability and stability of the piezoresistive effect as well as the durability of sensing devices at that nano level is still controversial [16,17]. Therefore, the enhancement of strain

* Corresponding authors.
E-mail addresses: congthanh.nguyen@griffith.edu.au (C.T. Nguyen), d.dao@griffith.edu.au (D.V. Dao).

https://doi.org/10.1016/j.apmt.2024.102157
Received 23 October 2023; Received in revised form 28 February 2024; Accepted 7 March 2024
Available online 11 March 2024

sensitivity at device scale still plays a critical role in this field. Table 1 summarizes the gauge factors of the most common bulk materials [18–20]. It is clearly noted that Si and Ge are the semiconductors of choice for large piezoresistive effect [21]. However, these low bandgap materials exhibit inherent problems at elevated temperatures [22]. In contrast to Si and Ge, silicon carbide (SiC) has a wider bandgap (2.3–3.2 eV), which leads to stable electrical characteristics at high temperatures [23,24]. The piezoresistive effect in SiC is also good with gauge factors of −31.8 and 30.3 for n-type and p-type 3C-SiC, respectively [20]. SiC also has great mechanical strength, high thermal conductivity, and strong chemical inertness, all of which are important for sensing devices operating in extreme environments [25,26]. Thanks to the advances in Si fabrication processes, single crystalline 3C-SiC has been successfully deposited on Si wafers with diameters up to 300 mm [27]. Consequently, commercially available 3C-SiC/Si wafers have been produced to meet the demands of academia and industry. Extensive studies on the strain-sensitive characteristics of 3C-SiC have been conducted, from the piezoresistive effect to the piezo-optoelectronic effect, from different fabrication possesses to novel sensor designs [8,28,29].

Mechanical stress also affects the electrical properties of p-n junction devices, which is known as the piezojunction effect [31,32]. The change in the current through the junction under an applied strain is caused by the alteration in the mobility of minority carriers and the concentration of intrinsic carriers [31]. For example, a uniaxial tensile bending stress induced an apparent increase in the base current while decreasing the collector current of bipolar transistors [31]. Based on this sensing effect, prototypes of some mechanical sensing devices have been developed, i.e., microphones, accelerometers, and pressure sensors [33–35]. Studying the piezojunction effect in Si and germanium (Ge) homojunctions, Wortman et al. reported that the stress level must be about $10^9 - 10^{10}$ dynes/cm^2 for utilizing these p-n junctions as stress transducers [36]. That stress level is close to the fracture strengths of Si and Ge, which explains why this effect has not been applied widely. According to the current literature, we note that the piezojunction effect in semiconductor heterojunctions has not been investigated. Therefore, as a proof of concept, this research used an n^+-3C-SiC/p-Si heterojunction for developing ultrasensitive mechanical sensing devices. Applying the beam bending method, the forward current was measured under different strain conditions. The obtained experimental results demonstrate the highly sensitive piezojunction effect in the SiC/Si heterojunction for pressure/strain sensing applications.

2. Device fabrication and experimental setup

Experiments were conducted using cantilevers constructed from a 3C-SiC/Si heterojunction to investigate the piezojunction effect under forward bias. The fabrication process encompassed ten main steps, Fig. 1. The starting material was a commercially available p-type silicon wafer, with the thickness of 400 μm and the doping concentration of 10^{14} cm^{-3}. Firstly, we cleaned the wafer following the RCA (Radio Corporation of America) cleaning procedure (Step 1). Following this, we grew an epitaxially single crystalline heavy-doped n^+-3C-SiC layer on top of the original Si wafer (Step 2). This epitaxial growth process was carried out with low-pressure chemical vapor deposition at 1000 °C using propene and silane precursors. The resulting 3C-SiC layer is approximately 500 nm ± 10 % thick, confirmed by NANOMETRICS Nanospec-based measurement. The transmission electron microscopy (TEM) image shows a crystal defect at the SiC/Si interface, Fig. 2a. The selected area electron diffraction (SAED) image confirms the single crystalline of 3C-SiC on the Si, Fig. 2b. The doping concentration of this SiC thin film is approximately 5×10^{18} cm^{-3}, confirmed by the hot probe and Hall effect methods. The back surface of the Si wafer was then sputtered with aluminium (Step 3), spin-coated with a photoresist layer (Step 4), and then patterned by exposure to ultraviolet light using the maskless aligner MLA150 from Heidelberg Instruments (Step 5). The same processes were applied to the SiC surface (Steps 6–8). The formation of top and bottom electrodes was achieved through wet etching (Step 9), then we diced the wafer into cantilevers of 40-mm length and 10-mm width (Step 10).

Fig. 2c illustrates the experimental setup for examining the strain-sensitive characteristics of the SiC/Si heterojunction under forward bias. The depletion region in the interface between SiC and Si is created by layers of positive and negative immobile ions resulting from the diffusion of majority charge carriers (electrons and holes) in opposite directions [37,38]. The cantilever was fabricated along two typical orientations [100] and [110] on the Si wafer (100). One end of the cantilever close to the vertically aligned electrodes was clamped while another end was subjected to varying loads. A forward bias was applied to the SiC/Si heterojunction through the fabricated electrodes using Keithley 2450 source meter. Specifically, the positive end of the source meter was connected to the top electrode on the SiC while the negative end was connected to the back electrode on the Si. All experiments were conducted in a dark condition at room temperature.

Table 1
Longitudinal gauge factors of the most common semiconductors.

Material	Orientation			Reference
	[100]	[111]	[110]	
n-Si	−133	−14	−52	[19,30]
p-Si	+8.6	+175	+120	[19,30]
n-Ge	−5.3	−157	−105	[19,30]
p-Ge	−10.9	+102	+65	[19,30]
n-GaAs	−3.2	−8.9	−6.7	[19]
p-GaAs	−12	+38.2	+21	[19]
n-3C-SiC	−31.8	–	–	[7,20]
p-3C-SiC	–	–	+30.3	[8,20]

3. Results and discussions

First, the current-voltage (I–V) characteristics of the SiC/Si heterojunction under free strain condition were examined, starting with the test of contacts between aluminum (Al) electrodes and their respective semiconductor layers. To do this, two electrodes on the same surface were connected to the source meter, then a voltage sweep from −3 V to 3 V was applied. The obtained I–V curves between lateral electrodes on the SiC layer and Si substrate are presented as Fig. 3a, and the linear I–V relationships demonstrate the excellent Ohmic contacts of the fabricated Al electrodes. This results in the extremely low resistance between these electrodes and their semiconductor layers, so the SiC/Si heterojunction chiefly decides the electrical behavior between the vertically aligned electrodes. Fig. 3b shows the excellent p-n junction characteristics under both forward and reverse biases. The current undergoes an exponential increase as a response to the applied forward bias while diminishing significantly under the reverse voltage.

Second, the piezojunction effect in the SiC/Si heterojunction under forward bias was experimentally investigated by using the beam bending method. Two typical orientations [100] and [110] with different Young's modulus were examined. Using a pulley to change the load direction, different loads from 10 g to 60 g were introduced to induce tensile or compressive strains in the SiC/Si cantilever. As the SiC thickness is much smaller than that of Si, the bending-induced strain in SiC is expected to be the same as the strain at the Si interface. Next, we determined the mechanical strain in the SiC layer as follows:

$$\varepsilon = \frac{Mt}{E_{Si}I} = \frac{6M}{E_{Si}wt^2} \quad (1)$$

where M is the applied moment, t is the thickness of the SiC/Si cantilever, E_{Si} is the Young's modulus of Si (130 GPa in [100] orientation and 169 GPa in [110] orientation), I is the inertial moment, and w is the width of the SiC/Si cantilever [39].

By applying a specific bias voltage, the change in the forward current

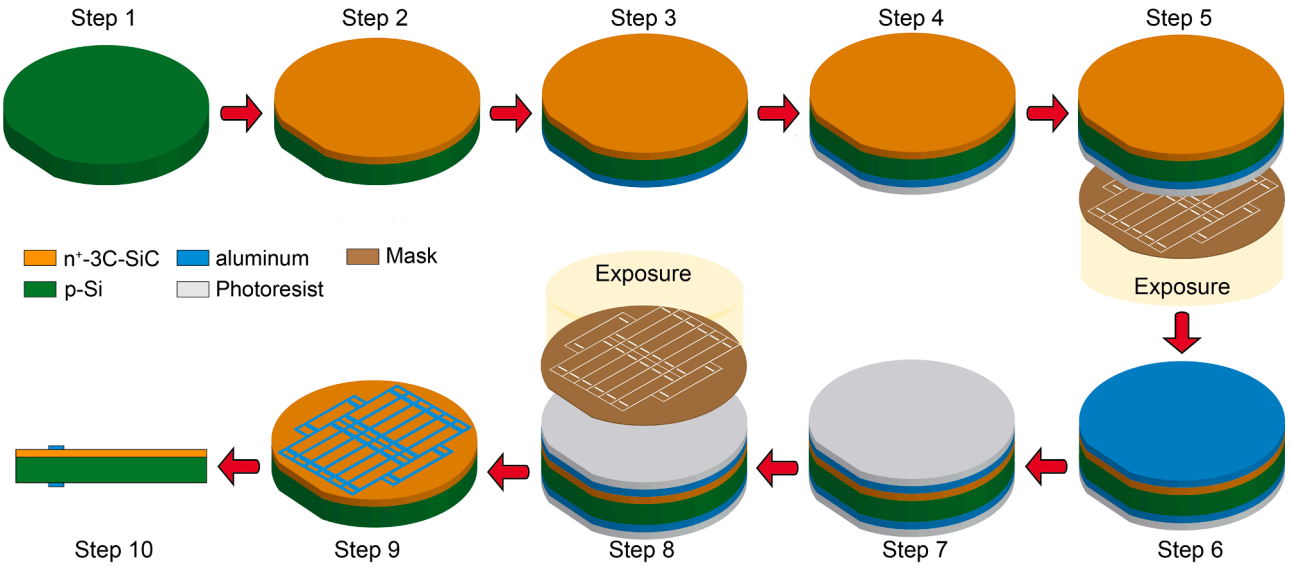

Fig. 1. Fabrication process. Step 1: Clean the commercial Si (100) wafer. Step 2: Grow a 3C-SiC thin film on top of the Si wafer. Step 3: Sputter Al on the back side. Step 4: Spin coat photoresist on the back side. Step 5: Photolithography the back side. Step 6: Sputter Al on the top side. Step 7: Spin coat photoresist on the top side. Step 8: Photolithography the top side. Step 9: Wet etch Al on both sides. Step 10: Dice the wafer into cantilevers.

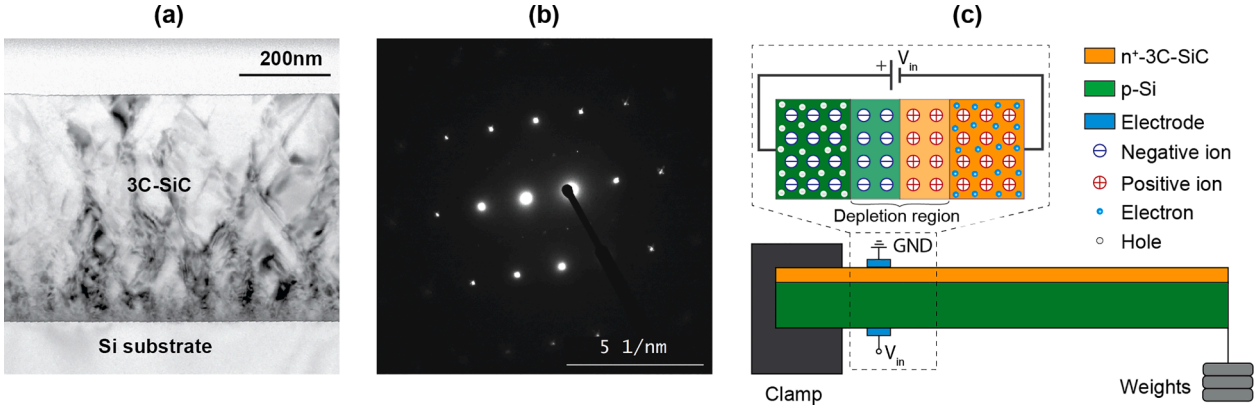

Fig. 2. (a) TEM image of the 3C-SiC. (b) SAED image of the 3C-SiC. (c) Schematic of the experimental setup.

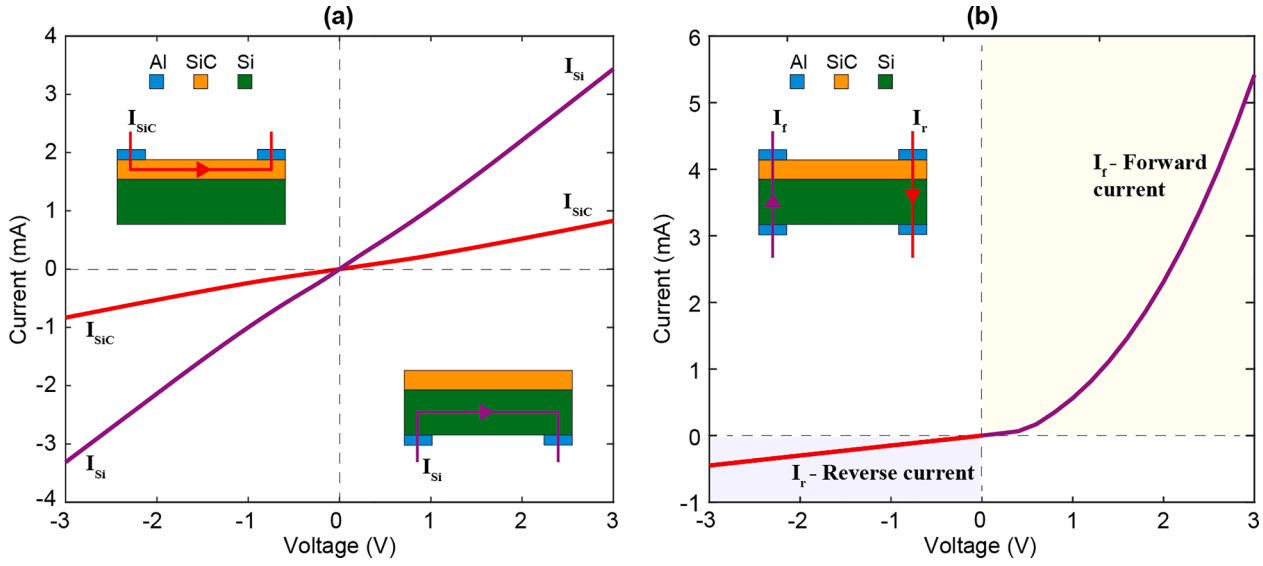

Fig. 3. Current-voltage characteristics of the fabricated device. (a) I–V curves between lateral 1-mm spacing electrodes on the SiC and Si surfaces, (b) I–V curve between the vertically aligned electrodes on top and bottom of SiC/Si heterojunction.

with respect to the varied strain application was measured by the four-point measurement using the source meter Keithley 2450. Fig. 4a,b present the change in the forward current under 4-V bias when hanging the cantilevers with different loads of 20, 40, and 60 g. It is clearly seen that the forward current decreases under tensile load but increases under compressive load for both [100] and [110] orientations. Taking the orientation [100] as an example, the forward current is 10.89 mA under free strain condition, going down to 10.62 mA under 60 g-tension load and going up to 11.20 mA under 60 g-compression load. The induced strain on the SiC layer beneath the top electrode was then computed. Fig. 4c clearly shows the linear relationship between relative current change ($\Delta I/I$) and induced strain from 0 to 500 ppm under the forward bias of 4 V, decreasing under tensile strain while increasing under compressive strain. We should note that the difference in Young's modulus of two orientations induces different strains under the same applied load. The fractional current changes under tension and compression were also symmetric for both [100] and [110] orientations. Furthermore, the relative current change for the [100] oriented cantilever is larger than that of the [110] oriented cantilever. These results indicate the ability of this piezojunction effect for developing mechanical strain/pressure sensors.

To evaluate the piezojunction effect in the SiC/Si heterojunction, gauge factor (*GF*)—the ratio between the factional resistance change and the induced strain was calculated as follows:

$$GF = \frac{\Delta R}{R_0} \times \frac{1}{\varepsilon} = \frac{-\Delta I}{I} \times \frac{1}{\varepsilon} \quad (2)$$

where ΔR is the resistance change, R_0 is the forward resistance under a free strain condition, ΔI is the current change, and I is the forward current under an applied strain.

Using (2), the *GFs* of the n^+-3C-SiC/p-Si heterojunction when bending along [100] and [110] orientations are 55.5 and 37.6, respectively. Interestingly, these *GFs* are positive while the *GFs* of n-3C-SiC thin film are known to be negative. Besides, these *GFs* are significantly higher than the highest longitudinal *GF* (− 31.8) of n-3C-SiC along the most sensitive [100] orientation reported in the literature [7].

Third, experiments were replicated with other forward biases from 2 V to 8 V. Fig. 4d shows the obtained gauge factor with respect to the applied bias. The inset depicts the SiC/Si wafer with two orientations [100] and [110] selected to fabricate the cantilevers. The most remarkable result to emerge from this figure is that the *GFs* increase exponentially when increasing the applied voltage. At 8-V forward bias, the *GFs* of the SiC/Si heterojunction when bending the [100] and [110] oriented cantilevers are 199.7 and 173.1, respectively. These values are about 630 % and 540 % higher than the highest longitudinal *GF* of n-3C-SiC along the most sensitive direction [100] reported to date in the literature. Besides, the orientation [100] is more sensitive with higher *GFs* than [110] under all applied voltages. Again, these results

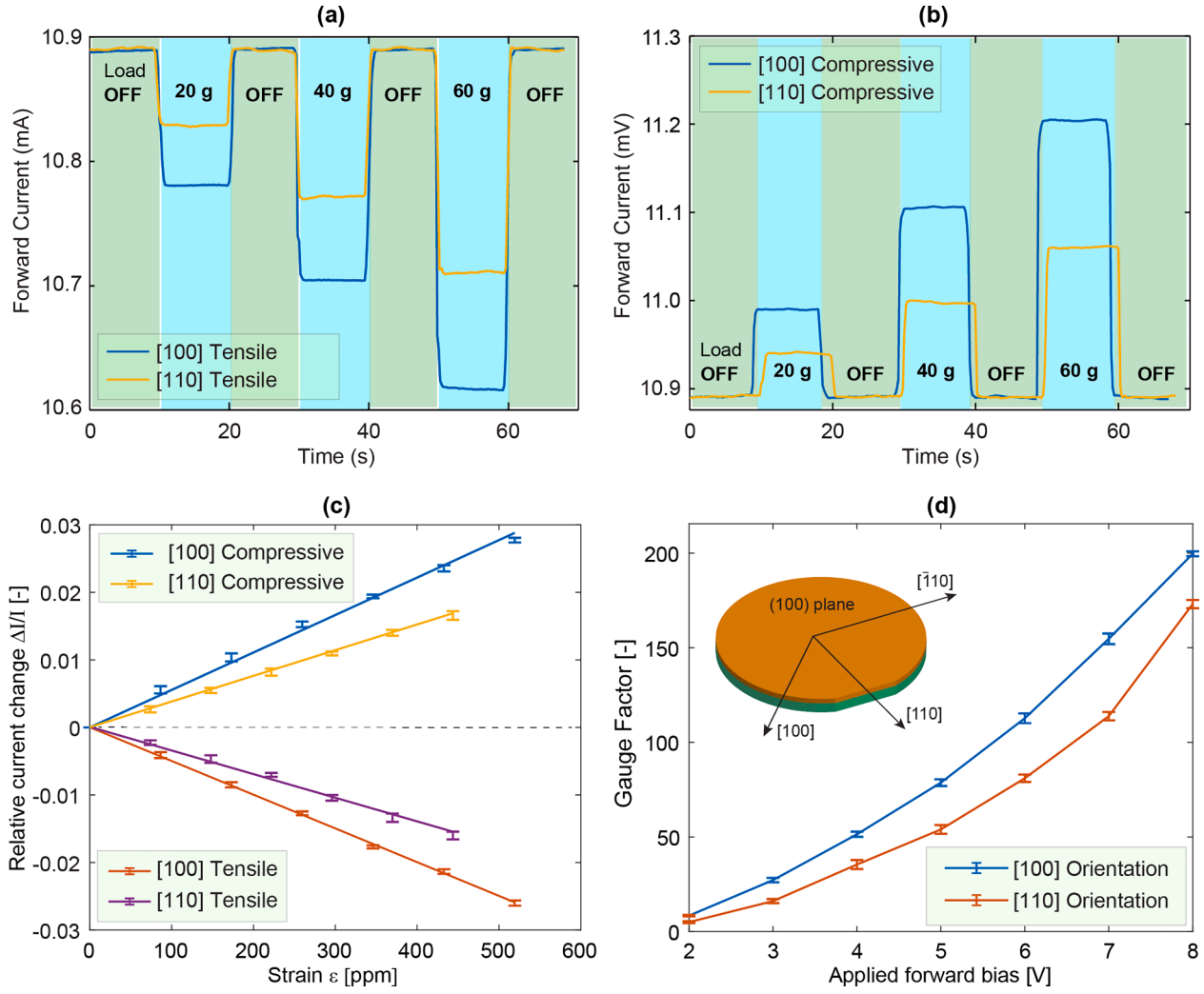

Fig. 4. The forward current at 4-V bias under (a) tensile conditions, (b) compressive conditions. (c) Responses of the fractional current change to the induced tensile and compressive strains at the forward bias of 4 V. (d) Responses of the gauge factor with respect to the applied forward bias.

demonstrate the ultrasensitive piezojunction effect in the SiC/Si heterostructure for mechanical sensor applications.

Fig. 5 explains in detail the ultrasensitive piezojunction effect in the SiC/Si heterojunction under forward bias. Applying a vertically downward load to the free end of the cantilever induces a tensile strain in the top SiC layer, which causes the conduction band split and consequently the repopulation of charge carriers, Fig. 5a [40,41]. The top right inset shows six equivalent energy valleys in the conduction band of n-type SiC under an unstressed condition. These ellipsoid valleys align with six-equivalent ⟨100⟩ orientations in k-space. In a single valley, the effective mass of an electron is oriented dependent or anisotropic. The larger energy curvature of the ellipsoid valley results in the smaller effective mass, which means the electron effective mass along the rotational axis is larger than that along the perpendicular direction ($m_{\parallel} > m_{\perp}$). We consider two of the six energy valleys along the orientations [100] and [001] to explain the piezojunction effect in this study. The applied strain is along [100] orientation, then the band structure and electron effective mass are considered in [001] direction or the out-of-plane direction through the junction. The induced tension results in the upward movement of the band edge ($+\Delta E$) along the direction [100] and downward movement of the band edge ($-\Delta E$) along the perpendicular direction [001] [1]. As electrons tend to transfer to the valley with a lower energy level, the repopulation reduces the number of electrons in the [100] valley while increasing electrons in the [001] valley. Consequently, when downwardly bending the cantilever along [100] orientation, less electrons exist with higher energy level in [100] valley, whilst more electrons with lower energy level are in [001] valley.

Fig. 5b depicts the energy band diagram of the SiC/Si heterojunction and the effective mass of electrons in 3C-SiC along the orientation [001] or out-of-plane direction when the [100] oriented cantilever is bent down. The stress state in the Si substrate changes continuously from tensile in the top half to compressive in the bottom half while the thickness of SiC is much smaller than the diffusion length of charge carriers. Therefore, the effect of these regions on the forward current under stress/strain can be ignored. Considering the area around the depletion region, the barrier height of valence bands (1.7 eV) is much larger than that of the conduction bands (0.45 eV). Consequently, the alteration in the forward current in the SiC/Si heterojunction under the applied load mainly results from the strain modulation on the migration of electrons from SiC to Si. Fig. 5a indicates that there are the same number of electrons in two perpendicular energy valleys under the unstressed condition. Considering the out-of-plane direction, the electrons

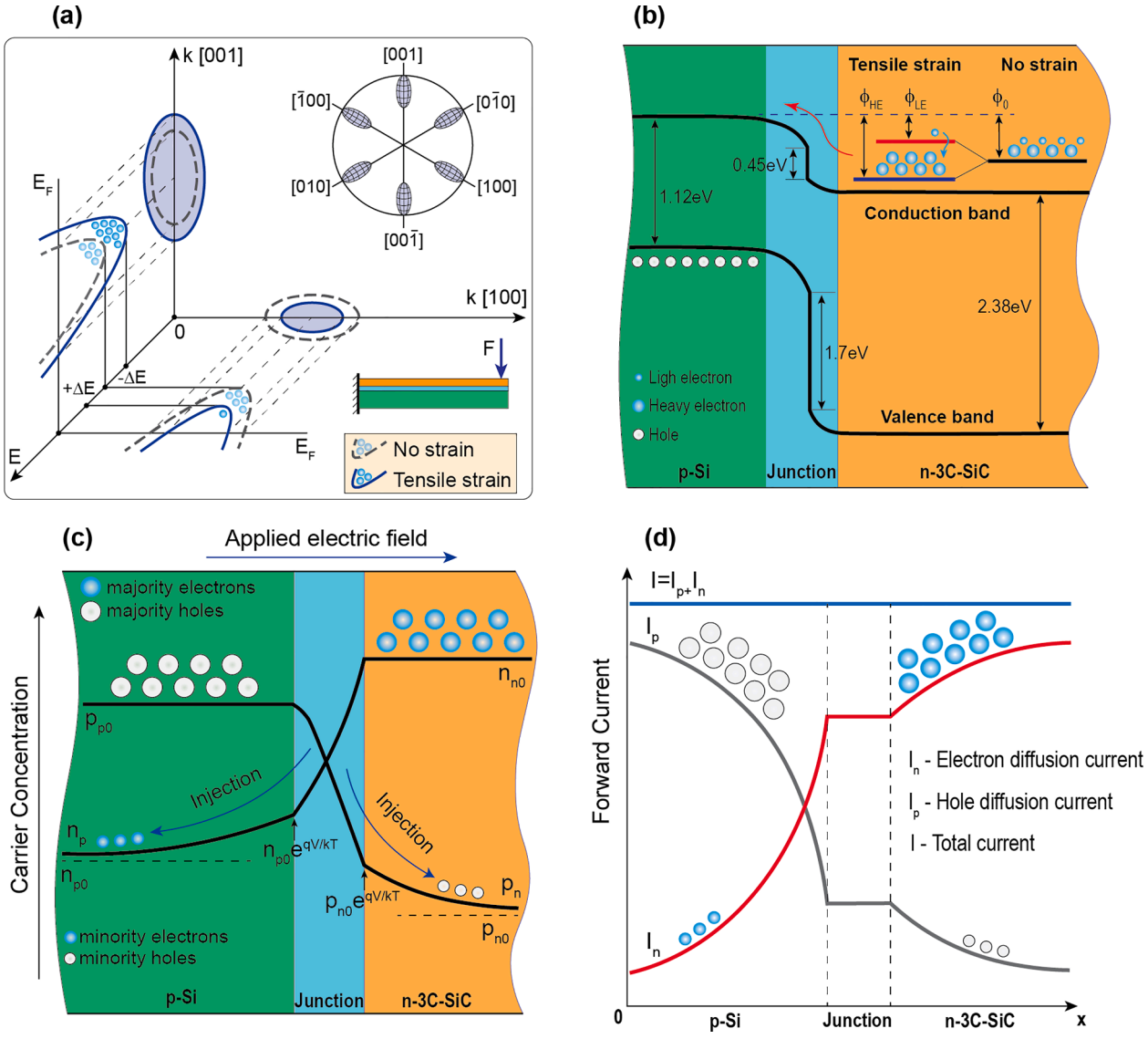

Fig. 5. Phenomena explanation. (a) Modulation of two n-SiC energy valleys in k-space under tensile strain, (b) Energy band diagram and effective mass of charge carriers along the out-of-plane direction under tensile strain, (c) Carrier distributions under forward bias, (d) Current densities under forward bias.

in the ellipsoid valley [001] are heavier than those in the valley [100] ($m_{\parallel} > m_{\perp}$). On the other hand, the tensile strain induces the band split and the electron repopulation, resulting in more heavy electrons ($m_{\parallel}$) with lower energy, and less light electrons ($m_{\perp}$) with higher energy. In other words, under tensile strain, there are more heavy electrons with larger energy barrier (ϕ_{HE}) and less light electrons with smaller energy barrier (ϕ_{LE}), reducing the average mobility or increasing the resistivity in the out-of-plane direction. This hypothesis is consistent with the decrease in the forward current under tension as obtained in experiments. In the case of compression, opposite strain effects on the band split and electron effective mass cause an increase in the forward current, which is again consistent with the corresponding experiments.

Fig. 5c and d present the idealized carrier distributions and current densities in the SiC/Si heterojunction under an applied forward bias. This bias voltage causes the injection of charge carriers in opposite directions, so minority electrons move toward the p-Si while minority holes migrate to the n^+-3C-SiC (Fig. 5c). However, the injected minority-carrier densities are relatively small in comparison with the majority-carrier densities. Taking into consideration the positions at the boundary of the depletion region on the p-Si and n^+-3C-SiC sides, the minority electron and hole densities are determined respectively as [38]:

$$n_p = n_{p0}\exp\left(\frac{qV}{kT}\right) \tag{3}$$

$$p_n = p_{n0}\exp\left(\frac{qV}{kT}\right) \tag{4}$$

where n_{p0} and p_{n0} are the equilibrium electron and hole densities on the p-Si and n^+-3C-SiC, respectively, q is the elementary charge, k is the Boltzmann constant, T is the temperature, and V is the applied forward bias.

Fig. 5d schematically illustrates the current densities in the SiC/Si heterostructure. The total current through the heterojunction is the sum of the electron and hole diffusion currents:

$$I = I_n + I_p \tag{5}$$

where I is the total current, I_n and I_p are the electron and hole diffusion currents. As the depletion width is much smaller than the diffusion length, the electron and hole currents throughout the depletion region are considered to be constant, which are calculated as follows [38]:

$$I_n = \frac{qD_n n_{p0}}{L_n}\left[\exp\left(\frac{qV}{kT}\right) - 1\right] \tag{6}$$

$$I_p = \frac{qD_p p_{n0}}{L_p}\left[\exp\left(\frac{qV}{kT}\right) - 1\right] \tag{7}$$

where D_n and D_p are the electron and hole diffusion coefficients, L_n and L_p are the electron and hole diffusion lengths, respectively.

The electron current is due to the injection from n^+-3C-SiC to p-Si, but its magnitude is determined by the properties of the p-Si (D_n, L_n, n_{p0}). On each side of the heterojunction, the total current is the sum of the majority and minority diffusion currents, which is constant throughout the heterojunction. In summary, the introduced forward bias changes the carrier distributions and current densities in the SiC/Si heterostructure. Furthermore, the increase in the applied forward voltage results in the reduction in the energy barrier and the decrease in the width of depletion region, Figure S3 [38]. In this case, the strain modulation on the electron effective mass and energy level influences significantly on the electron injection from n^+-3C-SiC to p-Si. In other words, the decrease in the barrier height and the reduction in the depletion region width under forward bias increase the strain sensitivity of the SiC/Si heterojunction. This explains the considerable enhancement of the piezojunction effect with large gauge factors under high forward bias.

All experimental results show that the *GFs* in [100] orientation are larger than those in [110] orientation under all applied voltages, Fig. 4. This is explained by the oriented dependence of the strain modulation on the effective mass and energy band of electrons in SiC. Specifically, the modulation along [100] orientation is more significant than the other direction. This was demonstrated by the piezoresistive effect in n-3C-SiC with a longitudinal *GF* of −31.8 in the orientation [100] compared to a longitudinal *GF* of −3.7 in the orientation [110] [7]. Consequently, the piezojunction effect obtains higher *GFs* when applying stress along the orientation [100].

4. Conclusions

This research reports the ultrasensitive piezojunction effect in a 3C-SiC/Si heterostructure under external bias. Cantilevers were fabricated along two typical orientations [100] and [110] using a wafer made of highly doped n^+-3C-SiC on low doped (100) p-Si substrate. Experiments were then conducted using the beam bending method, the forward current through the p-n junction was measured between two vertically aligned electrodes for comparison. Experimental results show a linear relationship between the relative current change and the induced strain from 0 to 500 ppm, decreasing with tensile strain and increasing with compressive strain. At the forward bias of 8 V, the obtained *GFs* when bending the [100] and [110] oriented cantilevers are 199.7 and 173.1, respectively. These values are about 630 % and 540 % higher than the highest gauge factor of n-3C-SiC along the most sensitive orientation [100] reported to date in the literature. It is also interesting to note that these *GFs* are positive whilst the *GFs* of n-3C-SiC thin films are known to be negative. The sensing effect was finally explained by a hypothesis based on the band split and mass shift of electrons under the strain modulation as well as the change in the barrier height, depletion region width, carrier concentration, and current density under forward bias. In conclusion, the demonstrated piezojunction effect in the SiC/Si heterojunction can pave the way toward the development of ultrasensitive mechanical sensors.

CRediT authorship contribution statement

Cong Thanh Nguyen: Conceptualization, Investigation, Data curation, Formal analysis, Writing – original draft. **Erik W. Streed:** Project administration, Funding acquisition. **Toan Dinh:** Writing – review & editing, Project administration, Funding acquisition. **Nam-Trung Nguyen:** Writing – review & editing, Project administration, Funding acquisition. **Van Thanh Dau:** Investigation, Writing – review & editing, Project administration, Funding acquisition. **Dzung Viet Dao:** Conceptualization, Investigation, Formal analysis, Writing – review & editing, Project administration, Funding acquisition.

Declaration of competing interest

The authors declare that they have no known competing financial interests or personal relationships that could have appeared to influence the work reported in this paper.

Data availability

The data are available from the corresponding author upon reasonable request.

Acknowledgments

This work was supported by the Australian Research Council under Discovery Projects (DP220101252). This work used the Queensland node of the NCRIS-enabled Australian National Fabrication Facility (ANFF). The 3C-SiC/Si material was developed and supplied by the Queensland Micro and Nanotechnology Centre, part of the Queensland

node-Griffith-of the Australian National Fabrication Facility, a company established under the National Collaborative Research Infrastructure Strategy to provide nano and microfabrication facilities for Australia's researchers. The sensing devices were also fabricated at the Queensland Micro and Nanotechnology Centre, Griffith University, Australia. The TEM and SAED images were implemented by Centre for Microscopy and Microanalysis, The University of Queensland, Australia. The authors would like to thank Mr. Khoi Le (School of Engineering and Built Environment, Griffith University) for valuable discussions. We are also grateful for all supports of research centres and research funds.

Supplementary materials

Supplementary material associated with this article can be found, in the online version, at doi:10.1016/j.apmt.2024.102157.

References

[1] Y. Kanda, Piezoresistance effect of silicon, Sens. Actuators A 28 (2) (1991) 83–91.
[2] L. Zhou, Q. Xin, J. Lin, S. Liang, G. Yang, A low-cost hydrogel with high conductivity and flexibility for pressure sensor and supercapacitor, Appl. Mater. Today 34 (2023), https://doi.org/10.1016/j.apmt.2023.101907.
[3] T.-K. Nguyen, et al., Highly sensitive 4H-SiC pressure sensor at cryogenic and elevated temperatures, Mater. Des. 156 (2018) 441–445, https://doi.org/10.1016/j.matdes.2018.07.014.
[4] L. Pan, et al., An ultra-sensitive resistive pressure sensor based on hollow-sphere microstructure induced elasticity in conducting polymer film, Nat. Commun. 5 (2014) 3002, https://doi.org/10.1038/ncomms4002.
[5] L. Gao, et al., Nano electromechanical approach for flexible piezoresistive sensor, Appl. Mater. Today 18 (2020), https://doi.org/10.1016/j.apmt.2019.100475.
[6] C.S. Smith, Piezoresistance effect in germanium and silicon, Phys. Rev. 94 (1) (1954) 42.
[7] J.S. Shor, D. Goldstein, A.D. Kurtz, Characterization of n-type beta-SiC as a piezoresistor, IEEE Trans. Electron. Devices 40 (6) (1993) 1093–1099.
[8] H.-P. Phan, et al., Piezoresistive effect of p-type single crystalline 3C-SiC thin film, IEEE Electron. Device Lett. 35 (3) (2014) 399–401, https://doi.org/10.1109/led.2014.2301673.
[9] M. Eickhoff, M. Stutzmann, Influence of crystal defects on the piezoresistive properties of 3C–SiC, J. Appl. Phys. 96 (5) (2004) 2878–2888.
[10] R.S. Okojie, A.A. Ned, A.D. Kurtz, W.N. Carr, Characterization of highly doped n- and p-type 6H-SiC piezoresistors, IEEE Trans. Electron. Devices 45 (4) (1998) 785–790.
[11] Y. Kanda, A graphical representation of the piezoresistance coefficients in silicon, IEEE Trans. Electron. Devices 29 (1) (1982) 64–70.
[12] A. Qamar, T. Dinh, M. Jafari, A. Iacopi, S. Dimitrijev, D.V. Dao, A large pseudo-Hall effect in n-type 3C-SiC(1 0 0) and its dependence on crystallographic orientation for stress sensing applications, Mater. Lett. 213 (2018) 11–14, https://doi.org/10.1016/j.matlet.2017.10.117.
[13] H.-P. Phan, et al., Thickness dependence of the piezoresistive effect in p-type single crystalline 3C-SiC nanothin films, J. Mater. Chem. C 2 (35) (2014) 7176–7179, https://doi.org/10.1039/c4tc01054j.
[14] A. Lugstein, M. Steinmair, A. Steiger, H. Kosina, E. Bertagnolli, Anomalous piezoresistance effect in ultrastrained silicon nanowires, Nano Lett. 10 (8) (2010) 3204–3208, https://doi.org/10.1021/nl102179c.
[15] R. He, P. Yang, Giant piezoresistance effect in silicon nanowires, Nat. Nanotechnol. 1 (1) (2006) 42–46, https://doi.org/10.1038/nnano.2006.53.
[16] A.R. Md Foisal, et al., Pushing the limits of piezoresistive effect by optomechanical coupling in 3C-SiC/Si heterostructure, ACS Appl. Mater. Interfaces 9 (46) (2017) 39921–39925, https://doi.org/10.1021/acsami.7b12128.
[17] J. Milne, A. Rowe, S. Arscott, C. Renner, Giant piezoresistance effects in silicon nanowires and microwires, Phys. Rev. Lett. 105 (22) (2010) 226802.
[18] A.S. Fiorillo, C.D. Critello, S.A. Pullano, Theory, technology and applications of piezoresistive sensors: a review, Sens. Actuators A 281 (2018) 156–175, https://doi.org/10.1016/j.sna.2018.07.006.
[19] K. Bethe, The scope of the strain gage principle, in: Proceedings. VLSI and Computer Peripherals. COMPEURO 89, IEEE, 1989, pp. 3/31–3/38.
[20] H.-P. Phan, D.V. Dao, K. Nakamura, S. Dimitrijev, N.-T. Nguyen, The piezoresistive effect of SiC for MEMS sensors at high temperatures: a review, J. Microelectromech. Syst. 24 (6) (2015) 1663–1677, https://doi.org/10.1109/jmems.2015.2470132.
[21] C.T. Nguyen, K.T. Nguyen, T. Dinh, V.T. Dau, D.V. Dao, Wearable physical sensors for non-invasive health monitoring. Wearable Biosensing in Medicine and Healthcare, Springer, 2024, pp. 111–132.
[22] D.P. Pham, D. Oh, V.-A. Dao, Y. Kim, J. Yi, Enhanced energy conversion performance of silicon solar cells by quantum-confinement effect of polysilicon oxide, Appl. Mater. Today 29 (2022), https://doi.org/10.1016/j.apmt.2022.101604.
[23] H. Xiong, et al., Characterizations on the doping of single-crystal silicon carbide, Mater. Today Phys. 29 (2022), https://doi.org/10.1016/j.mtphys.2022.100906.
[24] X. Qian, P. Jiang, R. Yang, Anisotropic thermal conductivity of 4H and 6H silicon carbide measured using time-domain thermoreflectance, Mater. Today Phys. 3 (2017) 70–75, https://doi.org/10.1016/j.mtphys.2017.12.005.
[25] N.H. Protik, A. Katre, L. Lindsay, J. Carrete, N. Mingo, D. Broido, Phonon thermal transport in 2H, 4H and 6H silicon carbide from first principles, Mater. Today Phys. 1 (2017) 31–38, https://doi.org/10.1016/j.mtphys.2017.05.004.
[26] C.T. Nguyen, et al., Photovoltaic effect-based multifunctional photodetection and position sensing using a 3C-SiC/Si heterojunction, ACS Appl. Electron. Mater. (2023), https://doi.org/10.1021/acsaelm.3c01145.
[27] L. Wang, S. Dimitrijev, J. Han, P. Tanner, A. Iacopi, L. Hold, Demonstration of p-type 3C–SiC grown on 150 mm Si (1 0 0) substrates by atomic-layer epitaxy at 1000 C, J. Cryst. Growth 329 (1) (2011) 67–70.
[28] H.-P. Phan, et al., The piezoresistive effect in top–down fabricated p-type 3C-SiC nanowires, IEEE Electron. Device Lett. 37 (8) (2016) 1029–1032, https://doi.org/10.1109/led.2016.2579020.
[29] T. Nguyen, et al., Giant piezoresistive effect by optoelectronic coupling in a heterojunction, Nat. Commun. 10 (1) (2019) 4139, https://doi.org/10.1038/s41467-019-11965-5.
[30] L.E. Hollander, G.L. Vick, T. Diesel, The piezoresistive effect and its applications, Rev. Sci. Instrum. 31 (3) (1960) 323–327.
[31] M. Hong, et al., Origin of current variations in ultrathin bipolar junction transistors under bending stress, IEEE Trans. Electron. Devices 70 (9) (2023) 4532–4537, https://doi.org/10.1109/ted.2023.3294463.
[32] J.J. Wortman, Semiconductor Piezojunction Transducers, NASA, 1968.
[33] M. Sikorski, Transistor Microphone, J. Audio Eng. Soc. 13 (3) (1965) 207–217.
[34] J. Wortman, L. Monteith, Semiconductor mechanical sensors, IEEE Trans. Electron. Devices 16 (10) (1969) 855–860.
[35] J. Matovic, Z. Djuric, N. Simicic, A. Vujanic, Piezojunction effect based pressure sensor, Electron. Lett. 6 (29) (1993) 565–566.
[36] J. Wortman, J. Hauser, R. Burger, Effect of mechanical stress on p-n junction device characteristics, J. Appl. Phys. 35 (7) (1964) 2122–2131.
[37] C.T. Nguyen, et al., Vertical piezo-optoelectronic coupling in 3C-SiC/Si heterostructure for self-powered and highly-sensitive mechanical sensing, ACS Appl. Mater. Interfaces (2023) 28781–28789, https://doi.org/10.1021/acsami.3c03045.
[38] S.M. Sze, Y. Li, K.K. Ng, Physics of Semiconductor Devices, John wiley & sons, 2021, p. 815.
[39] H.-P. Phan, et al., Fundamental piezoresistive coefficients of p-type single crystalline 3C-SiC, Appl. Phys. Lett. 104 (11) (2014) 111905.
[40] C. Herring, E. Vogt, Transport and deformation-potential theory for many-valley semiconductors with anisotropic scattering, Phys. Rev. 101 (3) (1956) 944.
[41] D.V. Dao, Study on Silicon Piezoresistive Six-Degree of Freedom Micro Force-Moment Sensors and Application to Fluid Mechanics, *Doctoral thesis*, Ritsumeikan University, 2003.